RSC Sustainability

ROYAL SOCIETY OF CHEMISTRY

PAPER

View Article Online
View Journal | View Issue

Cite this: *RSC Sustainability*, 2024, **2**, 3981

Unifying *Candida antarctica* lipase B and nZVI in bioinspired polymer nanomicelles: a nanobiohybrid synergy for sustainable synthesis of acetaminophen†

Falguni Shukla, Dilraj Singh and Sonal Thakore *

Polymer micelles are tailored nanostructures with the unique ability to encapsulate hydrophobic molecules that have proven to be promising candidates for applications such as drug delivery. With an aim to utilize the robust nature of polymer micelles for catalysis, we have synthesized a novel amphiphilic polymer derived from biocompatible precursors, such as tyrosine and polyethylene glycol. The polymer subsequently self-assembles into nanomicelles. These nanomicelles were loaded with *Candida antarctica* lipase B (CALB) and zerovalent iron nanoparticles (nZVI). The final magnetic catalyst (nZVI-CALB@NM) served as a nanoreactor for a one-pot cascade reaction consisting of two sequential steps, *i.e.*, hydrolysis and reduction in an aqueous medium. The cascade synthesis of *p*-aminophenol from a series of *p*-nitrophenyl esters of fatty acids with different chain lengths was attempted in one pot at 35 °C in an aqueous medium. The hydrolysis step was catalyzed by CALB and the reduction step was catalyzed by nZVI synergistically in the hydrophobic core of nanomicelles to achieve the final product in high yield. Further, to demonstrate the industrial application of the nanoreactors, we have carried out the synthesis of acetaminophen, which is a commercial bioactive molecule. The cascade synthesis of *p*-acetaminophen from *p*-nitrophenylacetate was achieved in a single pot within 30 min without an acid catalyst and organic solvent in excellent yield (>98%). Recycling studies demonstrated the possibility of utilizing the catalyst possessing magnetic properties for five successive cycles without any significant loss of activity. The main advantages of our system are the solubility of hydrophobic substrates in an aqueous medium and superior catalytic activity, leading to a significant reduction in the consumption of toxic solvents, reaction time, and temperature compared to those previously reported. The as-prepared nanoreactors will open up a new avenue for other chemoenzymatic reactions in the future by combining the enzyme and metal catalyst.

Received 24th July 2024
Accepted 20th October 2024

DOI: 10.1039/d4su00412d

rsc.li/rscsus

Sustainability spotlight

We have successfully unified *Candida antarctica* lipase B (CALB) and nano zero-valent iron (nZVI) within bioinspired polymer nanomicelles, creating a nanobiohybrid system that can revolutionize the sustainable synthesis of acetaminophen. This innovative strategy leverages the high selectivity and catalytic efficiency of CALB with the powerful reduction capabilities of nZVI encapsulated in environmentally friendly polymer nanomicelles.

1 Introduction

Enzymes are used as biocatalysts for a broad range of chemical transformations and have recently drawn increased attention due to their specific catalytic activities.[1–3] Efficient recovery and cycle time of enzymes are crucial for organic transformations at a larger scale to ensure the practical applicability and sustainability of a process.[4] Hence, enhancing the stability and recyclability of enzymes requires their engineering, before their use at a commercial scale.[5,6] Among enzymes, lipases (triacylglycerol ester hydrolases, EC 3.1.1.3) are an important member of the hydrolase family.[7] Lipase B from *Candida antarctica* (CALB) was selected for this study due to its well-documented catalytic versatility and stability under various reaction conditions. CALB is known for its high specificity and efficiency in catalyzing esterification, transesterification, and hydrolysis reactions, making it an ideal candidate for complex cascade reactions. Additionally, its robustness and compatibility with a wide range of substrates and solvents further enhance its suitability for incorporation into nanoreactors. These properties ensure that CALB can effectively function within the designed polymer micelles, facilitating efficient and

Department of Chemistry, Faculty of Science, The Maharaja Sayajirao University of Baroda, Vadodara 390 002, India. E-mail: chemistry2797@yahoo.com; sonal.thakore-chem@msubaroda.ac.in

† Electronic supplementary information (ESI) available. See DOI: https://doi.org/10.1039/d4su00412d

sustainable chemical transformations. Commercially available lipase, *viz. Candida antarctica* lipase B (CALB), is utilized for hydrolysis of fatty acid esters, esterification and transesterification reactions.[8] Given the importance of enzyme stability and recyclability for practical applications, integrating enzymes with metal nanoparticles into nanobiohybrid systems presents a promising strategy to enhance their catalytic efficiency and operational longevity.

Nano-biohybrid systems are known to rationally combine metal nanoparticles (chemocatalysts) that possess a superior surface-to-volume ratio and an abundance of rich active surface atoms with the enzymes.[9] They form the basis of chemoenzymatic catalysis in which at least one enzyme and one metal catalyst are involved.[10–12] This combines the broad reactivity of the heterogeneous chemocatalyst with the selectivity of the enzyme. Additionally, enzymes act as scaffolds that help to stabilize metal nanoparticles, preventing their migration and agglomeration during catalysis.[13] This establishes a synergism between enzymes and nanoparticles to enhance the catalytic potential.

To date, nanobiohybrids such as highly dispersed ultrasmall precious metal nanoparticles (Ag, Au, Pd or Pt) generated *in situ* and embedded in the CALB protein structure in aqueous media and at room temperature are synthesized.[9] Compared to noble metals, low-cost metals such as iron-based nanohybrids offer cost-effective alternatives for catalytic application.[14] For instance, Palomo and coworkers reported the synthesis of ultrathin CALB protein iron(II) carbonate nanorods heterogenous bionanohybrid for oxidation, reduction and C–C coupling reactions.[15] Zerovalent iron nanoparticles (nZVI) possess excellent magnetic properties and are easy to synthesize with a large specific surface area, reusability and separability.[16] Hence, they demonstrate the potential to combine with enzymes to obtain nanobiohybrid materials for catalysis. The integration of nZVI and enzymes into a single platform will provide a better alternative for recycling enzymes and metal nanoparticles, which is crucial from an application perspective. Such platforms offer unique advantages such as close spatial distance between the enzyme and metal, enhanced catalytic efficiency, recyclability, mass transfer and synergism. Additionally, the agglomeration of magnetic nanoparticles, enzyme denaturation, metal catalyst deactivation and lack of recyclability can be prevented.[17]

There are very few reports on the integration of metal and enzyme on supports such as organic frameworks and surfactant micelles.[18,19] Compared to these supports, polymer micelles offer advantages such as tailored synthesis, biocompatible precursors and the possibility of chemical functionalization.[20] Polymeric micelles, essentially amphiphilic polymers self-assembled into nanomicelles *via* non-covalent interactions, are an attractive platform. With a simple core–shell structure, it creates a nano environment separated from incompatible bulk media and typically functions as a nanoreactor for the reactions to occur.[21] These nanoreactors can co-house both enzyme and metal catalysts in the hydrophobic core. Additionally, the amphiphilic nature of these self-assemblies resolves the solubility issues of substrates and catalysts in water.[22] This compartmentalization in the hydrophobic pockets of these nanoreactors increases the proximity between the substrate and the catalytic sites.[23] The convergence of nanohybrids and micellar catalysis will enable new features and foster sustainable catalysis. Polymer micelles have not been used for their integration, especially, to catalyze a cascade reaction to synthesize pharmaceutically important compounds.

A key highlight of this study is the innovative design of nanoreactors using amino acid-based polymer micelles, which effectively encapsulate both *Candida antarctica* lipase B (CALB) and nanoscale zero-valent iron (nZVI). This dual encapsulation within a biocompatible, self-assembling polymer matrix enhances catalytic efficiency and streamlines the synthetic process for compounds such as *p*-aminophenol and *p*-acetaminophen. The approach significantly reduces solvent usage and waste, promotes a high atom economy, and simplifies workup procedures by minimizing synthetic steps. This represents a substantial advancement in sustainable and efficient chemical synthesis methodologies.

2 Experimental section

2.1 Materials and methods

Boc-L-tyrosine methyl ester (99.0%), poly(ethylene glycol)methyl ether, (mPEG, $M_n = 5.0$ kg mol^{-1}), hexamethylene diisocyanate (HMDI), undecanoic acid (99%), trifluoroacetic acid (TFA), 1,4-diazabicyclo[2.2.2] octane (DABCO), phosphate buffer saline tablets (for preparation of pH 7.4 buffer solution), *Candida antarctica* lipase B (CALB), *p*-nitrophenyl acetate, *p*-nitrophenyl butyrate, *p*-nitrophenyl palmitate, *p*-nitrophenyl octanoate, *p*-nitrophenyl decanoate, *p*-nitrophenyl chloroformate and dialysis membrane (MWCO 3500 Da) were purchased from Sigma Aldrich, Mumbai, India. Various solvents (acetonitrile, *N*,*N*-dimethylformamide (DMF), dimethyl sulfoxide (DMSO), acetone and dichloromethane (DCM)) were obtained from Sisco Research Laboratories, Mumbai, India. Other reagents were of analytical grade, purchased from commercial sources, and used as received without further purification. The solutions were prepared using de-ionized water. The reaction temperature was controlled using a constant temperature bath equipped with a thermocouple probe.

2.1.1 Instrumentation. Nuclear magnetic resonance (^{1}H NMR) spectra were recorded on a Bruker Avance 500 MHz spectrometer using DMSO-d_6 as the solvent and tetramethyl silane as the internal standard. Fourier transform infrared spectroscopy (FTIR) measurements were performed using a Bruker Alpha IR spectrophotometer. The samples were ground with KBr and turned into pellets by disc pressing. The spectra were recorded in the 400–4000 cm^{-1} range. Using a TGA 2950 instrument, thermogravimetric analysis of the polymer was carried out from 25 to 750 °C under flowing N_2 (30 mL min^{-1}) with a heating rate of 10 °C min^{-1}. For high-resolution transmission microscopy (HR-TEM), the diluted polymer, CALB and nZVI-loaded polymer solutions were dispersed on carbon-coated copper grids. The sample-coated copper grids were then air-dried overnight at ambient temperature, and the concentrations of all the samples were maintained at 0.05 mg mL^{-1}. The images of the

samples were then recorded using a Jeol (Jem-2100F) electron microscope at an accelerating voltage of 200 kV. A JSM-7600 F field emission scanning electron microscope was used to characterize the morphology. The samples for Field Emission Gun Scanning Electron Microscopy (FEG-SEM) characterization were treated by spraying a thin platinum layer on their surface under vacuum conditions to enhance their conductivity. Dynamic light scattering (DLS) was determined using a Malvern Zetasizer (Nano-ZS 90), and the samples were maintained at 0.1 mg mL^{-1} for analysis. Atomic Force Microscopy (AFM) was performed using NTEGRA PRIMA, NT-MDT, Russia. The sample was maintained at 0.05 mg mL^{-1} for analysis. All the samples were dialyzed properly before the analysis. The iron concentration in the nanoreactors was measured with a simultaneous inductively coupled plasma (ICP) spectrometer, ARCOS, SPECTRO Analytical GmbH, Germany. The sample was acid digested for analysis. Ultraviolet-visible spectrophotometric determinations were performed using a PerkinElmer Lambda 35. Fluorescence spectra scanned on a JASCO FP-6300. X-ray photoelectron spectroscopy (XPS) was performed using an ESCA spectrometer (SPECS Surface Nano Analysis GmbH, Germany) to investigate the surface compositions and oxidation states. Vibrating sample magnetometer (VSM) analysis was performed using VSM 7410, Lakeshore, Sweden, at room temperature. Circular Dichroism (CD) analysis was performed using a J 815(JASCO) spectrometer to investigate the structural changes in free CALB and encapsulated CALB. All the samples were prepared in a DMSO : H_2O mixture and dialyzed to obtain a micellar solution for the characterization. High Performance Liquid Chromatography (HPLC) was performed on Shimadzu LabSolutions fitted with a UV detector. A 1 g mL^{-1} solution of acetaminophen (Sigma) in methanol was used as standard. Thin Layer Chromatography was used to check the deprotection of the NH_2 group of Boc-L-tyrosine methyl ester under a given reaction condition. The solvent system used was hexane : ethyl acetate (8 : 2).

2.2 Synthesis of tyrosine-derived amphiphilic polymer

The general strategy for the synthesis of amphiphilic polymers from tyrosine involved functionalization with hydrophilic mPEG segments *via* urethane linkage and hydrophobic alkyl side chains *via* amide linkage. This introduces appropriate amphiphilicity into the polymer structure and subsequently leads to the self-assembling of nanomicelles in an aqueous medium.

2.2.1 PEGylation of Boc-protected tyrosine (Boc-tyrosine-mPEG) (step 1). A solution of Boc-L-tyrosine methyl ester (0.500 g, 1.6 mmol) and mPEG (0.2 g, 0.004 mmol) in DMF (10 mL), HMDI (200 μL) was added under stirring at 200 rpm. DABCO (5.0 mg) was added as a catalyst, and the reaction proceeded at 60 °C for 3 h. The insoluble white product formed was separated from the reaction mixture by filtration using Whatmann 41 filter paper. The filtrate obtained was reprecipitated in water to obtain a white solid and separated by vacuum filtration, followed by washing with acetone and diethyl ether. The resulting solid was dissolved in 10 mL DMSO and further purified by dialyzing the polymer solution using a dialysis membrane (MWCO 3500 Da) against water to remove the low-molecular weight polymers. The purified polymer solution was lyophilized to obtain a white polymer and stored under vacuum until further use. The yield was (0.562 mg polymer) 70%.

^{1}H NMR (500 MHz, DMSO-d_6): δ 8.5 (1H, NH amide of Boc), 7.6 (1H, –NH of urethane), 7.3–6.6 (4H, –CH aromatic protons of tyrosine), 5.7 (2H, –CH_2 directly attached to –NH of urethane), 4.15–4.06 (1H, CH proton of tyrosine), 3.7 (3H, –CH_3 proton of methyl ester), 3.61 (2H, –CH_2 protons of tyrosine), 3.51–3.02 (–OCH_2, –OCH_3 characteristic peak of mPEG), 2.9–1.33 (–CH_2 protons of HMDI) and 1.45 (–CH_3 protons of Boc).

FTIR (KBr pellet, wavenumber (cm^{-1})): 3336 (N–H stretch), 2933, 2858 (C–H stretch aromatic) 1740 (C=O of methyl ester), 1686 (C=O of urethane), 1626 (C=O of Boc), 1572 (C–N of amide), and 1230 (C–O of ester).

2.2.2 Deprotection of Boc-tyrosine-mPEG (step 2). In a 25 mL round bottom flask, PEGylated Boc-L-tyrosine-methyl ester (0.5 g) was dissolved in 5 mL of dried DMSO, to which 4 mL of TFA was added and magnetically stirred at 200 rpm for 1 h at 0–5 °C. Then, the reaction mixture was stirred at 37 °C for 1 h. TFA was removed from the reaction mixture using a rotary evaporator, the polymer was further purified by dialyzing against water using a dialysis membrane (MWCO 3500 Da) for 24 h, and then the sample was lyophilized to obtain yellowish-colored powder. The yield was (0.360 g polymer) 72%.

^{1}H NMR (500 MHz, DMSO-d_6): 8.5 (1H, –NH of urethane), 7.1–7.4 (–CH aromatic protons of tyrosine), 5.7 (2H, –CH_2 directly attached to –NH of urethane), 4.15–4.06 (1H, CH proton of tyrosine), 3.0 (2H, free amine), 3.61 (2H, –CH_2 protons of tyrosine), 3.4–3.5 (1H, –OCH_2 characteristic peak of PEG), and 1.2–1.33 (–CH_2 protons of HMDI).

FTIR (KBr pellet): wavenumber (cm^{-1}): 3345 (N–H stretch), 2934, 2861 (C–H stretch aromatic), 1739 (C=O of ester), 1707 (C=O of urethane), and 1216 (C–O of ester).

2.2.3 Conjugation of Tyr-mPEG polymer with undecanoic acid *via* amide bond formation (step 3). The product obtained (100 mg) in step 2 was dispersed in DMF in a 25 mL round bottom flask; undecanoic acid (100 mg, 0.53 mmol) was added, and the reaction mixture was sonicated for 15 min. EDC·HCl (1-ethyl-3-(3-dimethyl aminopropyl) carbodiimide hydrochloride) (100 mg) and NHS (*N*-hydroxy succinimide) (10 mg) were added, and the reaction was kept under magnetic stirring at 200 rpm overnight at room temperature. The product was filtered to remove the byproducts and reprecipitated in cold water. The product was separated by vacuum filtration and washed with water, followed by acetone. The polymer was dialyzed for further purification. The obtained product was dried and weighed. The yield was (0.150 g polymer) 75%.

^{1}H NMR (500 MHz, DMSO-d_6): δ (ppm) 8.5 (1H, –NH of urethane), 7.1–7.4 (–CH aromatic protons of tyrosine), 5.7 (2H, –CH_2 directly attached to –NH of urethane), 4.15–4.06 (1H, CH proton of tyrosine), 5.1 (1H, –NH of amide), 3.7 (3H, –CH_3 proton of methyl ester), 3.61 (2H, –CH_2 protons of tyrosine), 3.4–3.5 (1H, –OCH_2 characteristic peak of mPEG), 1.2–1.48 (–CH_2 protons of HMDI), and 2.77–2.99 (–CH_2 proton of undecanoic acid).

FTIR (KBr pellet): wavenumber (cm^{-1}): 3334 (N–H stretch), 2929, 2855 (C–H stretch aromatic) 1740 (–C=O of ester), 1688 (–

C=O of urethane), 1623 (–C=O of amide), and 1230 (C–O of ester).

2.3 Self-assembly of amphiphilic polymer into micelles and determination of critical micelle concentration

The micelles were prepared from the tyrosine-derived amphiphilic polymer by applying the solvent exchange method. Briefly, 10 mg of the amphiphilic polymer was dissolved in 10 mL of DMSO (1 mg mL^{-1} concentration). The solution was stirred at 200 rpm and 37 °C for 1 h and then dialyzed extensively against water using a dialysis membrane (MWCO 3500 Da). The critical micelle concentration (CMC) was determined by fluorescence spectrophotometry using pyrene as a probe. To determine CMC, the polymer concentration was varied from 1.0×10^{-5} mg mL^{-1} to 0.1 mg mL^{-1} with a concentration of pyrene fixed at 1.0×10^{-3} M. For the fluorescence study, an aliquot of 30 μL was drawn from each solution and diluted with distilled water, and the spectra were then recorded at an excitation wavelength of 330 nm. The emission fluorescence intensities at 373 and 384 nm were monitored. The point of intersection obtained after extrapolating the intensity ratio I_{373}/I_{384} in the high and low concentration regions was designated as the CMC value of the synthesized amphiphilic polymer.

2.4 Synthesis of catalytic nanoreactors (nZVI-CALB@NM) for chemoenzymatic reaction

2.4.1 Step 1: synthesis of CALB-loaded nanomicelles (CALB@NM). For the synthesis of CALB-loaded micelles, 12.5 mg of CALB was dispersed in 5 mL of PBS buffer and then slowly added to the nanomicellar solution (1 mg mL^{-1}) dropwise. The resulting solution was stirred for 5 h on a magnetic stirrer and then incubated at 4 °C for 2 h, followed by dialysis using (MWCO 3500 Da) against 100 mL of PBS buffer (10 mM, pH = 7.0). The final 10 mL of the solution obtained after purification by dialysis contained the desired CALB-loaded nanomicelles (CALB@NM).

2.4.2 Step 2: synthesis of zerovalent iron nanoparticle-loaded CALB@NM. To prepare nZVI-CALB@NM, 10 mL $FeCl_3$ solution (0.3 M) was sonicated for 10 min. Then, 10 mL $NaBH_4$ (0.8 M) solution was added dropwise for 10 min to the $FeCl_3$ solution under inert conditions with N_2 purging. The reaction mixture was sonicated for 30 min to ensure the complete reduction of Fe^{3+} ions to zero-valent iron (Fe^0) nanoparticles. To this reaction mixture, sodium hydroxide was added dropwise to adjust the pH to 8, followed by sonication for 10 min. The synthesized iron nanoparticles were separated by magnetic decantation, followed by washing with methanol and acetone thrice to remove excess borohydride and byproducts. Next, CALB@NM solution (10 mL) was added dropwise, and the resultant solution was stirred for 30 min under an inert condition with N_2 purging. The reaction mixture was subjected to dialysis against 100 mL of PBS buffer (10 mM, pH = 7.0). The obtained product was then stored in a refrigerator and characterized.

2.5 Determination of *Candida antarctica* lipase B loading in polymer nanomicelles

The amount of lipase binding to the nanomicelles *via* hydrophobic interactions was determined by the Bradford assay.[24,25] Loading of CALB was performed by applying the dialysis method.[26] For this purpose, 5 mg of polymer and 12.5 mg of CALB were taken in DMSO (5 mL), and Milli-Q water (5 mL) was added to this solution dropwise and stirred for 4 h. The solution was transferred to a dialysis bag of MWCO 3500 Da and dialyzed for 24 h against 150 mL of PBS buffer (10 mM, pH = 7.0) to remove the unencapsulated enzyme. Fresh PBS was replenished periodically. The dialyzed transparent solution was preserved, and the dialysis media was subjected to Bradford assay to determine the protein concentration. The calibration curve of BSA was plotted, as shown in Fig. S12.† The BSA loading capacity of the nanomicelles and their entrapment efficiency can be calculated by determining the BSA present in the dialysis media using a UV-visible spectrophotometer. All the experiments were carried out in triplicate. The loading capacity of the total protein was calculated using the following equation (eqn (1)):

$$\text{Loading capacity } (\%) = \frac{\text{total protein} - \text{protein in dialysis media}}{\text{total weight of polymer}} \times 100 \quad (1)$$

Entrapment efficiency can be calculated as the ratio of protein present in the polymer to the total weight of protein taken in the polymer, as follows:

$$\text{Entrapment efficiency } (\%) = \frac{\text{total protein} - \text{protein in dialysis media}}{\text{total protein content}} \times 100 \quad (2)$$

2.6 Amount of zerovalent iron nanoparticles loading in nZVI-CALB@NM`

The amount of zerovalent iron nanoparticles loading in the nanomicelles was determined from the iron content analyzed by Inductively Coupled Plasma Atomic Emission Spectroscopy (ICP-AES), after the acid digestion of the sample. For this protocol, 10 mg of polymer and 50 mg of synthesized zerovalent iron nanoparticles were taken in DMSO (5 mL), and Milli-Q water (5 mL) was added to this solution dropwise and stirred for 6 h. The solution was transferred to a dialysis bag of MWCO 3500 Da and dialyzed for 24 h against 250 mL of PBS buffer (10 mM, pH 7.0) to remove the unencapsulated iron. Fresh PBS was replenished periodically. The dialyzed transparent solution was preserved, and the dialysis media was utilized for the ICP-AES analysis.

2.7 Hydrolytic activity of nZVI-CALB@NM

The hydrolytic activity of the catalyst was determined using *p*-nitrophenyl acetate (*p*-NPA) as a substrate. In the enzyme activity assay, 50 μL of *p*-NPA (100 mM) and 2 mL of nZVI-CALB@NM (nanoreactors) were incubated at 35 °C using a constant temperature bath equipped with a thermocouple

probe. An aliquot of 30 μL was drawn from the reaction mixture at a fixed time interval and diluted with 2.5 mL of distilled water. The release of *p*-nitrophenol (*p*-NP) was then monitored using a UV-vis spectrophotometer (Agilent Cary 60) at a wavelength of 312 nm for 30 min at 35 °C.

2.8 Catalytic activity of nZVI-CALB@NM towards reduction of 4-nitrophenol

The catalytic activity of the nZVI-CALB@NM was measured using *p*-NP as a substrate. To optimize the reaction conditions for the reduction of *p*-NP, we performed the reactions in a cuvette. For the reaction, 50 μL aliquot of the sample was diluted in 450 μL of distilled water containing catalyst (18 wt% nZVI) and $NaBH_4$. The reaction progress was monitored using a UV-vis spectrophotometer. The absorption peak at 405 nm was observed due to the formation of intermediate nitrophenolate ions.

The time required for the completion of the reaction was monitored by scanning the UV spectrum at a fixed time interval of 1 min. As the reaction progresses, the absorbance at 405 nm decreases gradually, and the new absorption peak at 300 nm increases due to the formation of the *p*-aminophenol (*p*-AP).

The rate of the reaction was evaluated by studying the kinetics of the reaction in terms of the concentration of *p*-NP. The rate constant k was determined for the reaction using the plot of $\ln(C_t/C_0)$ *vs.* reduction time as per the following equation (eqn (3)):

$$\ln\left(\frac{C_t}{C_0}\right) = -kt, \tag{3}$$

where C_t is the concentration of the *p*-NP at time t (min), C_0 is the initial concentration of *p*-NP at time $t = 0$ (min) and k is the rate constant. The conversion of *p*-NP was calculated using the following equation (eqn (4)):

$$\text{Conversion} = \ln\left(\frac{A_t}{A_0}\right) \times 100\%, \tag{4}$$

where A_t denotes the UV absorbance at 405 nm, which is proportional to the concentration of the reduced *p*-NP, and A_0 is the initial UV absorbance at 405 nm after the addition of $NaBH_4$.

2.9 Multistep catalytic synthesis of acetaminophen using nZVI-CALB@NM

The synthesis of acetaminophen was carried out in a one-pot by mixing 18 mg of *p*-NPA substrate with nZVI-CALB@NM in a final reaction volume of 2 mL. Subsequently, 50.5 mg of $NaBH_4$ was added to initiate the reduction reaction. To measure the release of *p*-NP from *p*-NPA, a UV-visible spectrophotometer with a wavelength ranging from 250 to 500 nm was used. The reduction of *p*-NP to *p*-AP was also monitored at 405 nm *via* UV-visible spectrophotometer for 10 min at 2 min intervals. Finally, 0.1 g of acetic acid was added to the reaction mixture. The formation of the final product was monitored at 5 min intervals for the next 20 min. All reactions were performed at a controlled temperature of 35 °C using a constant temperature bath equipped with a thermocouple probe. For all UV measurements, 50 μL aliquots of the sample were diluted in 450 μL of distilled water.

2.10 Recycling studies

The catalyst and the product were separated after the reaction completion by simple extraction with chloroform (3 × 2 mL). After separation, the aqueous layer containing the nanoreactors was washed with diethyl ether to remove any organic molecules. Then, the solution was dialyzed extensively and reused for the next cascade cycle.

3 Results and discussion

3.1 Synthesis of tyrosine-derived amphiphilic polymer

For the synthesis, commercially available Boc-L-tyrosine methyl ester was used as a precursor, as shown in Scheme 1. Tyrosine was selected as the backbone of the polymer skeleton due to its multifunctionality and inherent biocompatibility. Our synthesis began with the functionalization with hydrophilic segment mPEG having a free hydroxyl group *via* urethane linkage using hexamethylene diisocyanate, resulting in pre-polymer 1.

To avoid the interference of the amine and carboxyl groups of tyrosine, the protected formed Boc-L-tyrosine methyl ester was used. The yield in all the steps was calculated with respect to the tyrosine derivative.

The formation of the urethane linkage between Boc-L-tyrosine methyl ester and mPEG was confirmed by the appearance of the characteristic peak of urethane at 7.6 ppm in the ^{1}H NMR (Fig. S1†). In FTIR analysis, a band for carbonyl at 1686 cm^{-1} corresponding to the urethane linkage was observed (Fig. S3†). Further, the Boc-protected amine of tyrosine was deprotected using trifluoroacetic acid to obtain pre-polymer 2 with a free amine group for further functionalization.[27] The deprotection of the Boc group of pre-polymer 2 was confirmed by ^{1}H NMR and FTIR analysis.

The disappearance of the peak at 1.38 ppm in NMR spectra and also the band around 1626 cm^{-1} corresponding to the carbonyl group of Boc moiety showed successful deprotection (Fig. S2 and S4†). To further confirm whether deprotection occurred under the given reaction conditions, Boc-L-tyrosine methyl ester was used as a model reactant. The reaction was carried out under similar reaction conditions and was monitored by thin layer chromatography. The product was isolated and confirmed by GC-MS analysis, which showed that the amine group was deprotected (as shown in Fig. S5†). Functionalization with undecanoic acid endows hydrophobic character to the polymer. Undecanoic acid was conjugated with the free amino group of pre-polymer 2 using 1-ethyl-3-(3-dimethylaminopropyl) carbodiimide as a reagent. The amidation was confirmed by FTIR analysis, which showed a carbonyl peak of amide around 1623 cm^{-1} (Fig. S6†). The structure of the final amphiphilic polymer was further confirmed by ^{13}C NMR (as shown in Fig. S7†). The characteristic peaks of urethane, amide and ester linkages were observed at 155.1, 174 and 176 ppm, respectively.

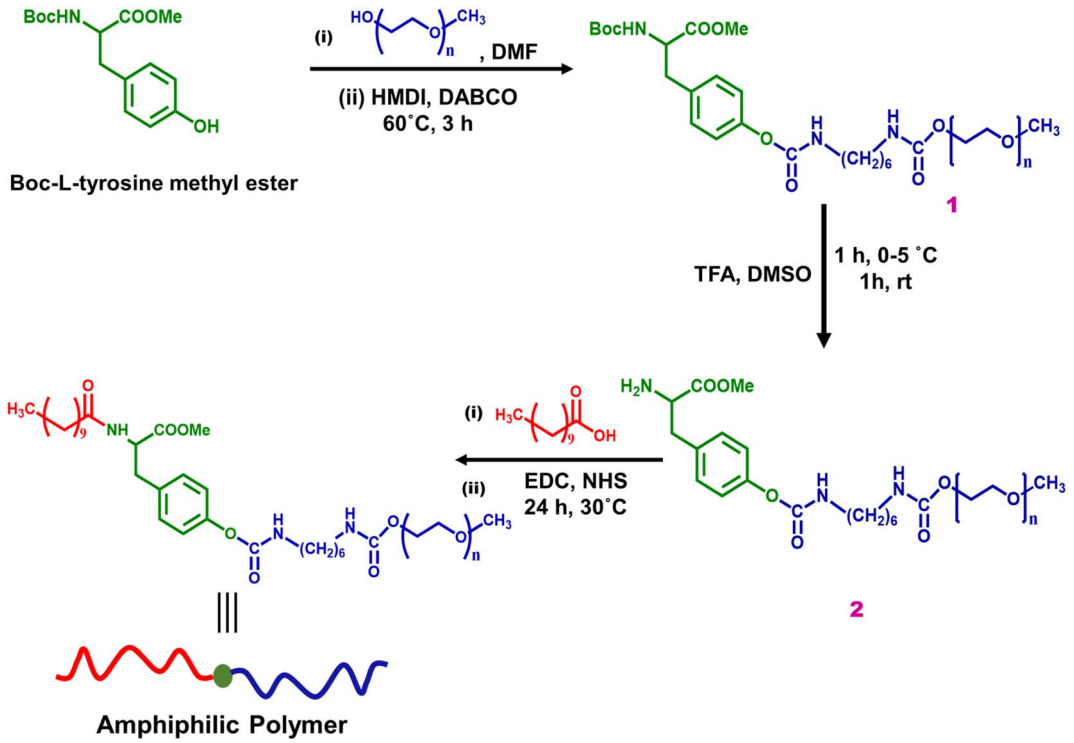

Scheme 1 Schematic of the synthetic route to poly(ethylene glycol) methyl ether, $M_n = 5000$, and undecanoic acid-tagged tyrosine amphiphilic polymer depicting the self-assembly of tyrosine amphiphilic polymer into nanomicelles.

The molecular weight (M_n) of the polymer was determined by applying the ^{1}H NMR end group analysis method. The amphiphilic polymer possesses $M_n = 7500$ g mol^{-1} shown in Fig. 1. TGA analysis of the final amphiphilic polymer revealed that the polymer was stable till 150 °C (Fig. S8†).

3.2 Self-assembly of tyrosine-derived amphiphilic polymers into nanomicelles

Amphiphilic polymers may self-assemble into aggregates with different structures, such as micelles, vesicles, rods, and hollow tubes.[28] The hydrophilic to hydrophobic ratio (HLB) plays a critical role in determining the morphology of the amphiphilic polymer. This is a useful feature for manipulating the morphology of an amphiphilic polymer for different applications involving catalysis. The nanomicelles were prepared from the amphiphilic polymer using the solvent exchange method.[29] To study the self-assembly of the tyrosine-derived amphiphilic polymer, the polymer sample was introduced into various solvents and their mixtures to obtain optimal conditions for the formation of the micelles. It was observed that the polymer sample when dissolved in DMSO + water and subjected to dialysis using a dialysis bag with MWCO 3500 Da obtained a stable aqueous clear polymer solution.

The critical micelle concentration value was determined using a hydrophobic dye, pyrene, as a fluorescent probe.[30] The nanomicelles exhibited a low CMC value of 0.97 mg L^{-1} (Fig. 2), which indicates that the synthesized amphiphilic polymer can form highly stable nanomicelles. This observation is supported by a well-known fact from the literature that the ratio of the hydrophobic portion in an amphiphile affects the CMC value. A smaller CMC value is attributed to the higher ratio of hydrophobic counterparts.[31] The hydrophobicity of the polymer was higher due to the aromatic ring of tyrosine, methyl groups of undecanoic acid present and methyl groups of HMDI present in the polymer skeleton. The relatively low CMC value makes the nanomicelles desirable candidates for catalytic application.

The self-assemblies were investigated by microscopic and spectroscopic studies to determine their morphology. For these studies, water insoluble fluorescent pyrene was chosen as model dye.[32] The pyrene was encapsulated in the polymer nanomicelles using the dialysis method.[26] First, the encapsulation of the pyrene was ensured from the florescence intensity of the extensively dialyzed solution, which had a characteristic emission peak of pyrene with $\lambda_{max} = 375$–405 nm, indicating successful dye encapsulation.[33] Further, to explore the micellar structure formed by self-assembly of newly synthesized amphiphilic polymer, a dye encapsulation study was carried out.[34] The dye-encapsulated solution showed the presence of single-layer blue emitting spherical micelles when examined under a florescence microscope (Fig. 2). This study confirmed the presence of a confined hydrophobic core inside the self-assembly as well as the ability of the aggregates to entrap hydrophobic guest molecules in its hydrophobic core.[35]

The morphology of the formed self-assembled nanomicelles was initially investigated using HRTEM. The HRTEM image of the bare nanomicelles showed the formation of spherical

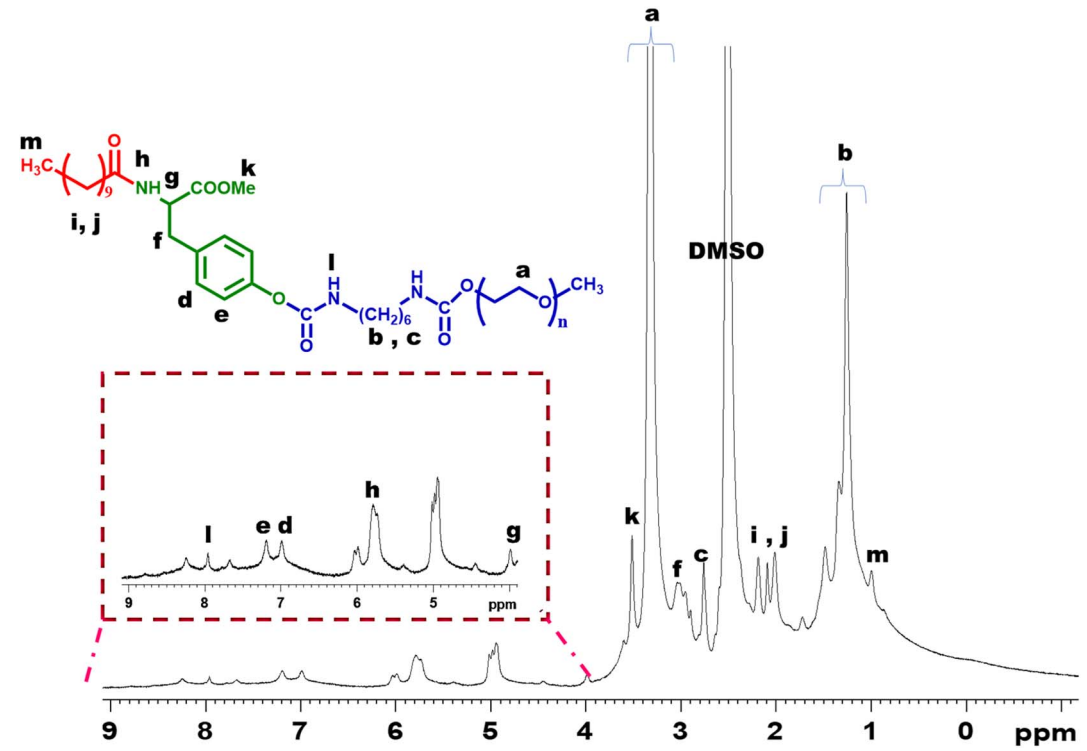

Fig. 1 ^{1}H NMR of the final amphiphilic polymer.

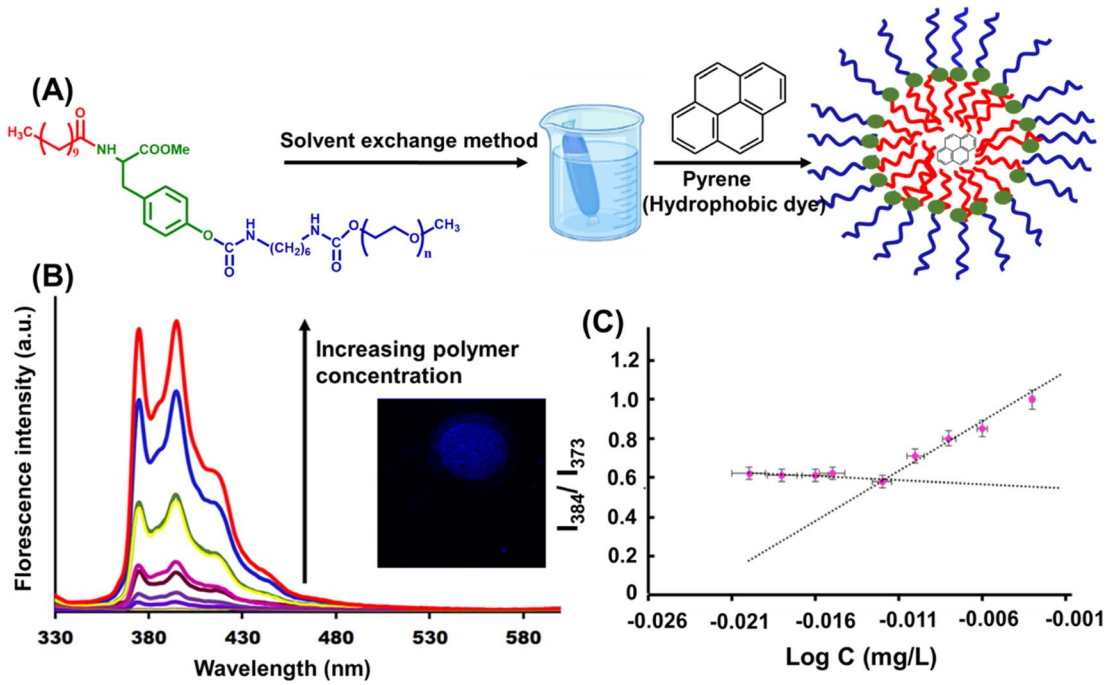

Fig. 2 (A) Schematic of the self-assembly of amphiphilic polymer into nanomicelles and subsequent encapsulation of pyrene dye (B) fluorescence emission spectra of pyrene as a function of polymer concentration varying from 1.0×10^{-5} mg mL^{-1} to 0.1 mg mL^{-1} (inset: fluorescence image of pyrene encapsulated micelles) and (C) determination of CMC using pyrene as a fluorescent probe. The data are presented as mean ± standard deviation of at least 3 independent experiments.

nanomicelles with an average diameter of 132 nm with a thin layer and core, which is clearly evident for the formation of nanomicelles (Fig. 3(A)). AFM is a very powerful tool for differentiating various nanoobjects. AFM analysis further confirmed the spherical morphology of the nanomicelles (Fig. 3(B)). The micellar aggregation of amphiphilic polymers

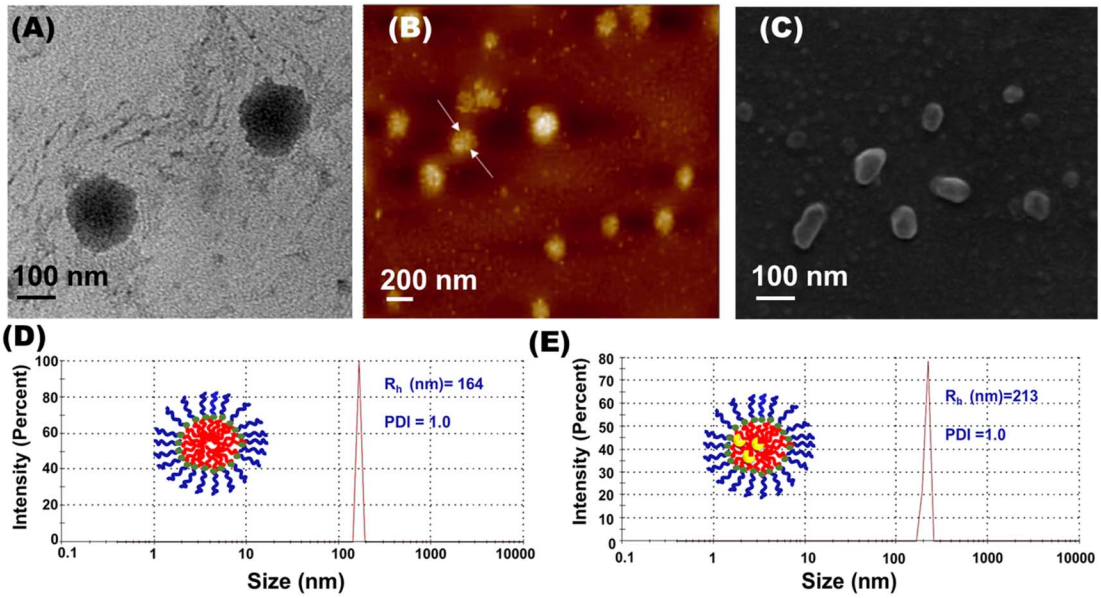

Fig. 3 Characterization of the self-assembly of tyrosine-derived amphiphile into nano micelles: (A) HR-TEM image; (B) AFM image; (C) FEG-SEM image (the samples were maintained at 1 mg mL^{-1} concentration for the above-mentioned characterizations), DLS. (D) Blank nanomicelles and (E) CALB-loaded nanomicelles (the samples were maintained at 0.1 mg mL^{-1}), [R_h: hydrodynamic radius].

was also confirmed by the FESEM investigation. The FESEM images showed spherical aggregates, corroborating the HRTEM results (Fig. 3(C)).

Dynamic Light Scattering (DLS) experiments were carried out to obtain the mean hydrodynamic radius and size distribution of the self-assembled bare nanomicelles. DLS analysis of this aqueous polymer solution exhibited mono-model distribution with good autocorrelation with respect to the formation of uniform size distribution of nano-aggregates of size 164 nm (Fig. 3(D)). The CALB-loaded nanomicelle samples also showed a mono-modal distribution with 213 nm size nanoobjects, indicating that the CALB is successfully loaded in the core of nanomicelles (Fig. 3(E)).

Based on the DLS studies and morphological characterization by HRTEM, AFM and FESEM, it can be confirmed that the newly synthesized tyrosine-derived micelles are very unique in retaining their micellar shape even after loading enzyme.

3.3 Synthesis of catalytic nanoreactors

We reported for the first time the successful design and synthesis of nanomicelles co-loaded with CALB and zerovalent iron nanoparticles to act as catalytic nanoreactors. The nanoparticles and enzymes are well dispersed in the hydrophobic core of the nanomicelles, avoiding their aggregation. The synthesis of the biohybrid was initiated by encapsulating CALB (1.2 mg mL^{-1}) in amphiphilic polymer-derived nanomicelles. The enzyme-loaded nanomicelle solution was dialyzed against PBS buffer (10 mM, pH = 7) to remove excess enzyme and calculate the quantity of enzyme loading in the nanomicelles. The CALB loading capacity and entrapment efficiency in the nanomicelles were 85% and 71%, respectively, calculated from eqn (1) and (2). The hydrodynamic size of the CALB@NM was 213 nm with uniform monodispersity. CALB hydrolyses the methyl ester from the amphiphilic polymer backbone, which results in free carboxylic acid groups, confirmed by a negative value (*i.e.*, −11.9 mV) obtained by the zeta potential analysis of the obtained dialysed solution (as shown in Fig. 4 and S9†). The obtained transparent dialysed solution was added to synthesize zerovalent iron nanoparticles for encapsulation. The free carboxylic group of tyrosine obtained after hydrolysis helps to stabilize iron nanoparticles *via* electrostatic interactions. The stable black dispersed solution was dialysed against PBS buffer (10 mM, pH = 7) to remove excess metal ions and was used as a catalyst. The loading of zerovalent iron nanoparticles was 18 wt% as estimated by ICP-AES analysis.

The catalytic nanoreactors were characterized by applying various techniques, such as HR-TEM, DLS, XPS and VSM. To establish the role of nanomicelles in stabilizing nZVI and CALB, HR-TEM imaging of nZVI-CALB was carried out in the presence and absence of nanomicelles (Fig. 5). HR-TEM micrographs of the nZVI-CALB in the absence of the nanomicelles showed an aggregated chain-like structure, in which the dark field contrast is due to nZVI and light field contrast is due to enzyme coating (Fig. 5(A) and (B)). HR-TEM micrographs of the nanoreactor confirmed the presence of spherical iron nanoparticles (Fig. 5(C)). The average particle diameter of the iron nanoparticles was found to be in the range of 10–15 nm. Moreover, the light field contrast was due to polymer nanomicelles that stabilized the iron nanoparticles. Notably, it is hard to distinguish between the polymer and CALB enzyme due to poor contrast under TEM mode.

Fig. 5(D) shows that, with the loading of zero valent iron nanoparticles and enzymes in the micelles, the average size of the formed micelles increases from 132 nm to 223 nm. A picture taken at higher magnification showed the spherical

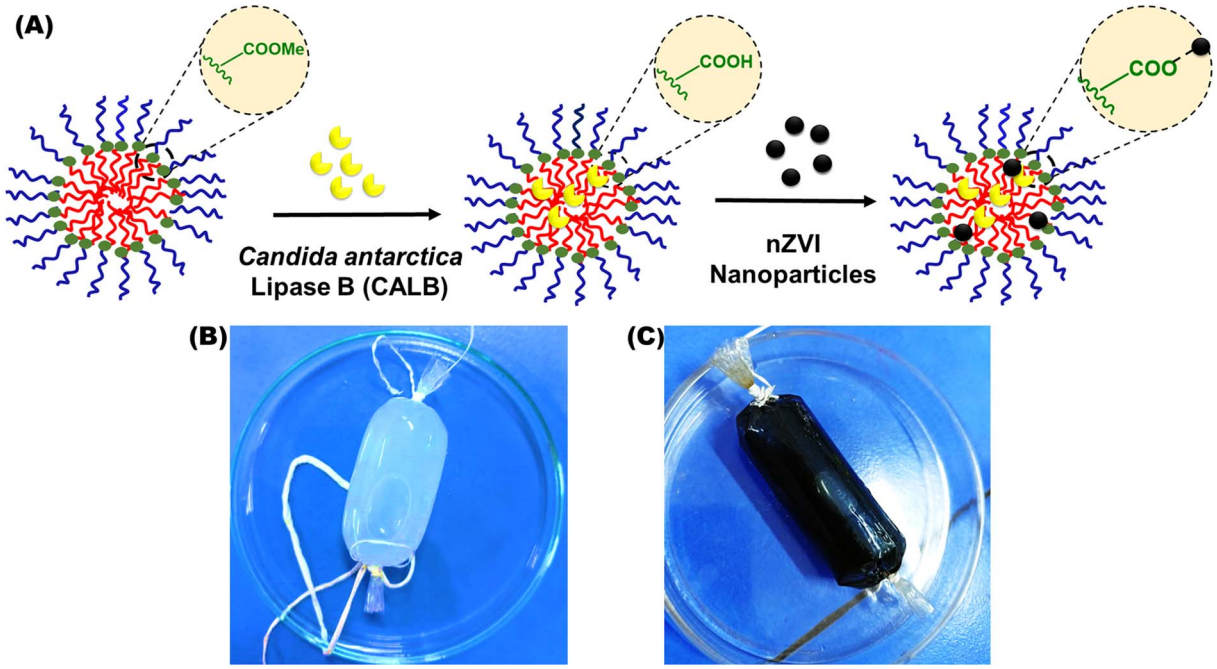

Fig. 4 Schematic of (A) CALB loading in nanomicelles leading to the hydrolysis of ester bond and subsequent loading of nZVI facilitated by free carboxyl groups, (B) CALB loading in nanomicelles (*i.e.*, CALB@NM) using dialysis method and (C) nZVI loading in CALB@NM using dialysis method, resulting in black coloured uniformly dispersed solution.

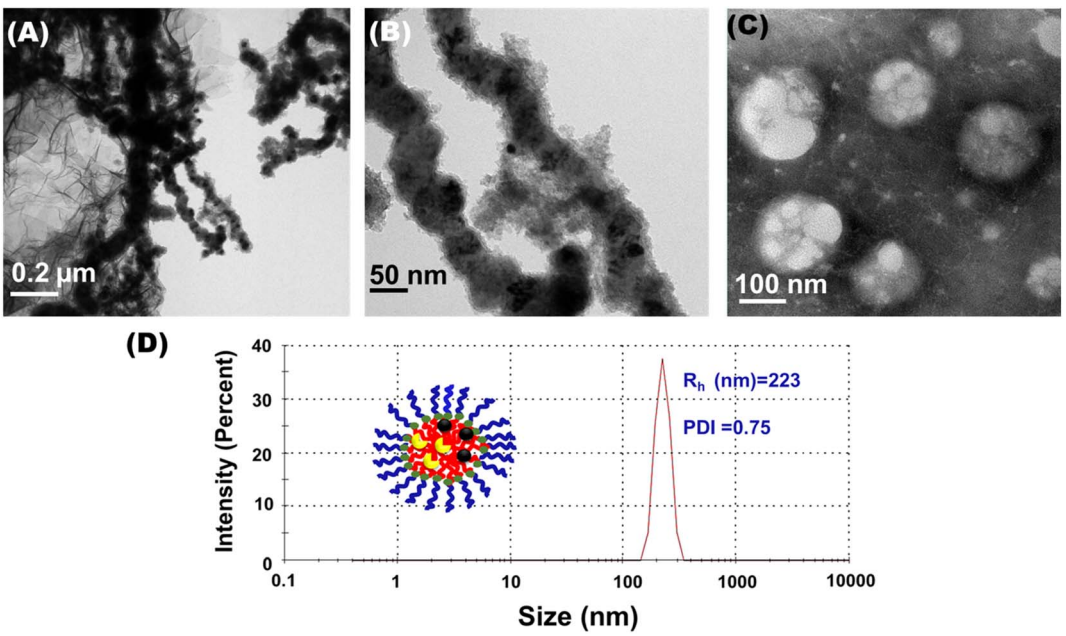

Fig. 5 Characterization of catalytic nanoreactors; HR-TEM images of CALB and nZVI (A); (B) in the absence of nanomicelles and (C) in the presence of nanomicelles (the samples were maintained at 1 mg mL^{-1} concentration for the above-mentioned characterizations.) and (D) DLS (the samples were maintained at 0.1 mg mL^{-1}), [R_h: hydrodynamic radius].

nanomicelles. TEM images also showed that clusters of spherical nZVI were observed in the micelles. The small size of nZVI leads to a high surface-to-volume ratio, which is advantageous for catalysis. The smaller size observed for nanomicelles in the HR-TEM measurements compared to the DLS studies can be attributed to the dehydration of the mPEG chains during sample preparation for the analysis.[36] The polydispersity was more pronounced in the TEM image of the nanoreactors analyzed on dried samples, where drying caused particle aggregation.[37] However, the TEM image (Fig. 5(C)) clearly showed spherical iron nanoparticles clustered in the hydrophobic cores of the micelles.

The surface composition of the catalyst was investigated by the XPS analysis. A complete scan from 0 to 1000 eV binding energy demonstrated the presence of C, O, N, and Fe in the catalyst (Fig. S10†). For XPS analysis, the catalyst was dried and then analyzed. The deconvoluted spectra of all the elements are shown in Fig. S11.† In the XPS analysis, the photoelectron could penetrate to a depth of about 5 nm below the surface, and the Fe^0 peak had a very low intensity. The intensity of the Fe^0 peak was found to be lower than the peaks of Fe 2p3/2 at 712.5 eV, corresponding to Fe(III) in the form of Fe_2O_3 and FeOOH, and at 719.1 eV, corresponding to the overlap of oxidized iron and zerovalent iron nanoparticles.[17] This can also be attributed to the oxidation of nZVI during the drying process. Thus, the low binding energy of 705 eV, corresponding to Fe(0), obtained was consistent with the literature.[38] The binding energies corresponding to the C 1s of the C–C and O–C=O linkages were observed at 284.8 and 288.6 eV, respectively. The binding energies for the 1s orbital of O were observed at 532 eV, corresponding to the C–O linkage, and 535 eV attributed to the metal oxide binding energy.[24] The binding energy for the 1s orbital of N was observed at 399 eV, which was attributed to the O=C–N linkage. Carbon, oxygen, and nitrogen were present due to the polymer nanomicelles in the nanoreactor composition.

To evaluate the magnetic properties of the loaded zerovalent iron nanoparticles, VSM analysis was carried out. The magnetic hysteresis curve is shown in Fig. S13.† The magnetization value was calculated as 24 emu g^{-1}. This confirms the superparamagnetic property, which is also evident from the easy separation using an external magnet.

To check the structural stability of native enzymes and enzymes loaded in nanoreactors, circular dichroism analysis was carried out. The CD spectra of native CALB and nZVI-CALB@NM show that the overall conformation of the CALB is intact in the two preparations. However, two spectra showed minor deviations, which can be due to some local conformational changes[39] (Fig. S14†).

3.4 Evaluation of nZVI-CALB@NM as a catalyst for chemoenzymatic cascade reaction

The nanoreactors were assessed for their catalytic activity towards the chemoenzymatic cascade reaction using *p*-NPA as a model reactant (Scheme 2). We started the experiments by referring to the values given in the prior literature in which similar reactions were performed using different catalytic systems.[24,40] Later, we selected the level range for each variable suitable for our experimental setup.

Initially, we carried out the reaction only in the presence of nanomicelles, in which *p*-NPA and sodium borohydride were added to the nanomicelle solution. It was observed that the reaction did not occur, and no change in the UV spectra was observed. This suggests that in the absence of an enzyme, hydrolysis of 4-NPA does not proceed. To understand the role of CALB and nZVI, the control reactions were also performed using enzyme-loaded micelles (CALB@NM) as catalysts. The UV-visible data revealed the formation of 4-NP from 4-NPA, which is due to hydrolysis in the presence of CALB, and the formation

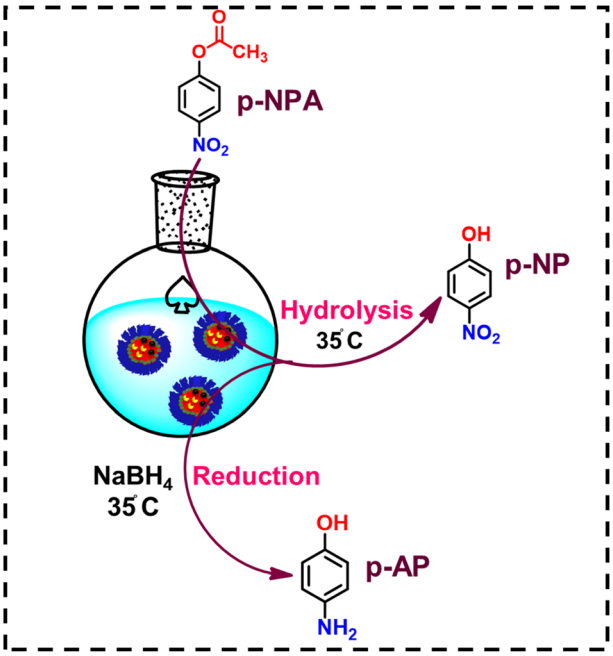

Scheme 2 Schematic of the chemoenzymatic cascade reaction in the presence of nZVI-CALB@NM.

of 4-AP does not occur in the absence of nZVI (Fig. S15†). These results revealed that the CALB plays a role in the hydrolysis of 4-NPA, and the nZVI with sodium borohydride is important for the final reduction step to obtain 4-AP as a product. Further, we carried out another set of control experiments to gain insight into the role of nanomicelles.

3.4.1 Advantage of using nanomicelles for the chemoenzymatic cascade synthesis of *p*-AP. To establish the role of nanomicelles, the hydrolysis and reduction reaction sequence was investigated using *p*-NPA as a substrate. Two sets of cascade reactions, one in the presence of nZVI-CALB@NM and another in the presence of a mixture of CALB-nZVI were performed.

3.4.2 Using nZVI-CALB@NM. First, when the reaction was performed in the presence of nanomicelles loaded with nZVI and CALB, no organic solvent was required to perform the reaction. The nanomicelles were capable of solubilising the substrate so that the reaction could be performed in an aqueous medium. Thus, the nanomicelles functioned as nanoreactors, and the nanomicelle solution acted as a reaction medium. The hydrolysis step, which marked the formation of *p*-NP, was successfully catalysed by the enzyme present in the nanoreactors. The completion of the hydrolysis step was observed in 15 min as confirmed by the UV spectra (discussed in Experimental section 2.9), and the hydrolytic activity was determined to be 85%. In addition to the reducing agent, sodium borohydride, a new peak was observed in the UV spectra corresponding to *p*-AP. This indicates that the nZVI in the nanoreactor catalyses the reduction of *p*-NP further to *p*-AP. The reduction step was completed in 10 min. Reaction kinetics for the reduction step was studied, and the k value was 15.8×10^{-2} min^{-1} with excellent conversion (>98%) (Fig. 6(A) and S16(A), (C)†).

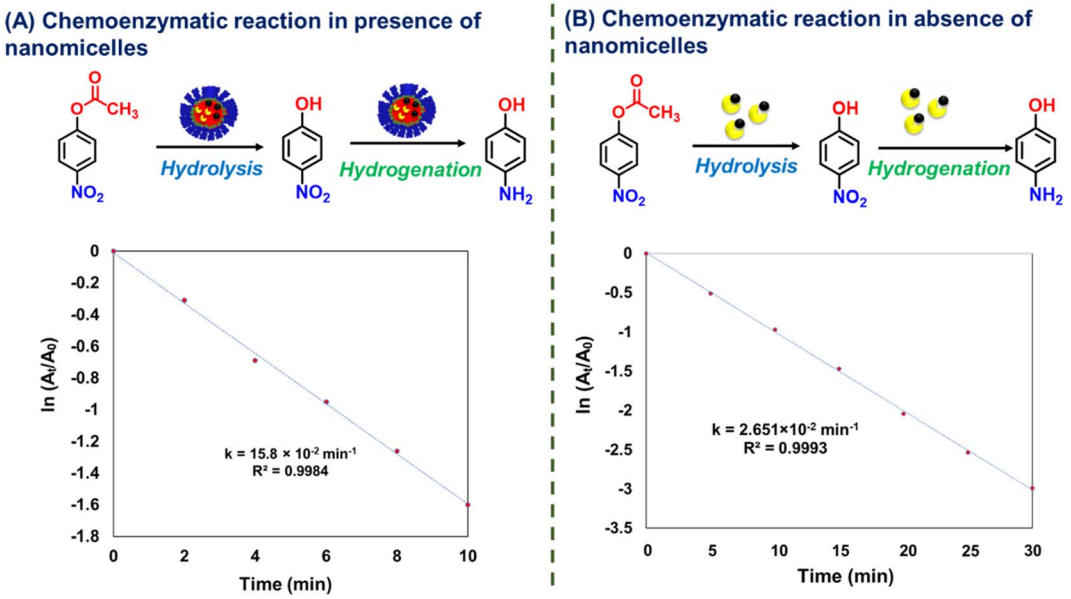

Fig. 6 Cascade synthesis of *p*-AP from *p*-NPA catalysed by nZVI-CALB and reaction kinetics of the reduction step (A) in the presence of nanomicelles and (B) in the absence of nanomicelles (reaction conditions: *p*-NPA (1 mM), catalyst (2 mL contains nZVI (18 wt%), $NaBH_4$ (1.4 mM) at 35 °C).

3.4.3 Using a mixture of nZVI-CALB in the absence of nanomicelles. The control cascade synthesis using the nZVI-CALB mixture as a catalyst in the absence of nanomicelles could not proceed in an aqueous medium. Owing to the insolubility of the substrate in water, it was performed in acetonitrile. The completion of the hydrolysis step took 25 min. The reduction step was completed in 30 min, and the k value was 2.65×10^{-2} min^{-1}. In this case, the whole cascade synthesis of *p*-AP required an hour, and the conversion obtained was 95% (Fig. 6 (B) and S15(B), (D)†).

These results clearly showed that in the presence of nanomicelles, the chemoenzymatic process demonstrated a higher catalytic activity in a lesser reaction time than in the absence of nanomicelles. Indeed, the presence of nanomicelles positively impacted the outcome of the chemoenzymatic reaction, leading to a faster reaction rate in water as a solvent.

3.5 Optimization of cascade reaction for the synthesis of *p*-AP

We investigated the chemoenzymatic cascade synthesis of *p*-AP from *p*-NPA under different reaction conditions. *p*-Nitrophenylacetate was used as the model substrate. As shown in Table 1, the volume of nanoreactors varied from 0.5 mL to 5 mL using sodium borohydride 2 mM with 1 mM *p*-NPA substrate

Table 1 Optimization of reaction conditions for the chemoenzymatic cascade catalysis for the synthesis of *p*-aminophenol using *p*-nitrophenylacetate as a model reactant[a]

Sr. No.	Volume of nanoreactors (mL)	Conc. of $NaBH_4$ (mM)	Conc. of Fe salt (M)	Conc. of *p*-NPA (mM)	Time (min)
1	0.5	2	0.1	1	40
2	1	2	0.1	1	35
3	2	2	0.1	1	20
4	3	2	0.1	1	20
5	5	2	0.1	1	18
6	2	1.8	0.1	1	25
7	2	1.6	0.1	1	26
8	2	1.4	0.1	1	26
9	2	1.2	0.1	1	30
11	2	1.4	0.2	1	15
12	2	1.4	0.3	1	10
13	2	1.4	0.4	1	10
14	2	1.4	0.5	1	8
15	2	1.4	0.3	5	12
16	2	1.4	0.3	10	20

[a] Reaction conditions: all the reactions were carried out at room temperature (35 °C).

concentration. For the cascade reaction, the time taken was 40 min and 35 min when 0.5 and 1 mL nanoreactors were used, respectively (Table 1, entry 1 and 2). When we increased the volume of the nanoreactors to 2 mL, the time required for the reaction completion was 20 min. Beyond 2 mL of nanoreactor volume, the reaction time did not change (Table 1, entry 4 and 5). Remarkably, enzymatic activity to hydrolyse the *p*-NPA was observed when 2 mL of micelle solution was used for the reaction.

Hence, the volume of the nanoreactors was fixed at 2 mL for further optimizations. Furthermore, the reduction step was performed using different concentrations of $NaBH_4$ in the standard reaction. When we decreased the concentration of $NaBH_4$ from 2 mM to 1.6 mM, the reaction time did not change (Table 1, entry 5–11), while using 1.4 mM of $NaBH_4$ resulted in a remarkable conversion, *i.e.*, 96% at 35 °C and reaction time, *i.e.*, 26 min (Table 1, entry 8).

Table 2 *p*-Nitrophenyl esters of fatty acids with different chain lengths tested for cascade reaction under the optimized condition using nZVI-CALB@NM[a]

Sr. No.	Substrate	Product	k ($\times 10^{-2}$ min^{-1})	% Conversion
1	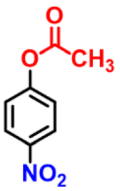	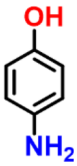	15.8	98
2	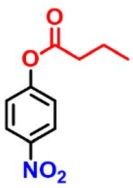	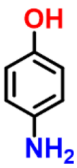	13.6	96
3	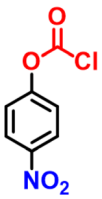	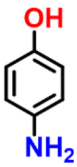	10.7	95
4	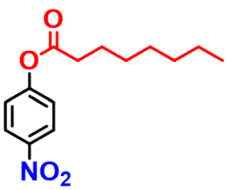	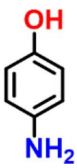	7.2	96
5	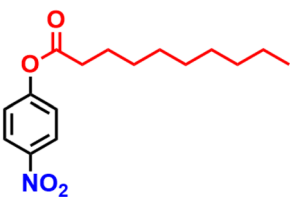	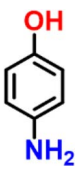	6.9	98
6	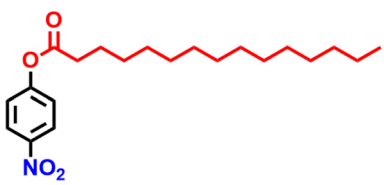	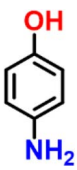	3.2	99

[a] Reaction conditions: substrates (1 mM), nanoreactors (2 mL, contains nZVI (18 wt%)), and $NaBH_4$ (1.4 mM) at 35 °C, and the % conversion was calculated using UV-visible spectrophotometry.

However, further lowering the concentration of $NaBH_4$ to 1.2 mM caused an increase in the reaction time (Table 1, entry 9); hence, an adequate concentration of $NaBH_4$ (1.4 mM) was used for the optimum reaction conditions. Further, we increased the iron loading in the nanomicelles by increasing the molarity of the iron salts from 0.1 M to 0.5 M. The reaction time decreased with increasing iron loading, as shown in Table 1, entry 9–14. The best result was obtained with 0.3 M iron. The optimum concentration of nZVI loaded was determined to be 18 wt% using ICP-AES analysis.

Further, under the optimized reaction conditions, the substrate concentration of *p*-NPA was increased from 1 mM to 10 mM. The reaction times for 1, 5 and 10 mM were 8, 12 and 20 min, respectively. Thus, the nanoreactors help to regulate the amounts of both the substrate and the product in aqueous media by providing a controlled supply that does not overload the enzyme, enabling greater conversion rates. Thus, nanomicelles help to control both substrate and product concentrations in an aqueous medium, allowing for higher rates of conversion.[19]

The reaction time was 10 min with 1.4 mM $NaBH_4$ and 2 mL of nanoreactor loading (Table 1, entry 12). On further increase in iron loading, no appreciable change in reaction time was observed.

After optimization of the reaction conditions, various *p*-nitrophenyl esters of fatty acids with different chain lengths were used as substrates. The hydrolysis and reduction of nitrophenyl esters proceed satisfactorily, affording a single product with good to excellent % conversion, which minimizes the efforts to separate the unreacted starting materials. The catalytic performance of nanoreactors was significantly influenced by the nature of the substituent on the nitroaromatic compound. The UV-visible spectra corresponding to the reduction of all the substrates in Table 2 are shown in Fig. S17.† The final product, 4-AP, formed from 4-NPA was also isolated and characterized by ^1H NMR, as shown in Fig. S18.†

p-Nitrophenyl esters with a long chain (Table 2, entry 4–6) require longer reaction times compared to the esters with a short chain substituent, which may be due to the increased hydrophobicity. The kinetics of the reduction step were investigated for every substrate, following a protocol similar to that mentioned above for *p*-NPA.

3.6 Synthesis of acetaminophen *via* sequential cascade catalysis in one pot

Several attempts have been made to synthesize paracetamol using different routes (Fig. 7). Generally, the commercial route begins with the nitration of benzene, which is associated with the formation of unwanted ortho aminophenol in significant amounts. Moreover, expensive platinum is required as a catalyst for the reduction step.

Many attempts have been made to replace corrosive and polluting sulphuric acid, but in some cases, the selectivities are low.[41] For instance, Gopinathan *et al.* synthesized acetaminophen with 86% yield from the hydroquinone and acetamide at elevated temperatures (280–300 °C) in the presence of solid acid catalysts, such as zeolite β or a heteropolyacid.[42] A green chemical route was proposed by Joncour and coworkers for the direct synthesis of acetaminophen with a high yield (95%) from hydroquinone using ammonium acetate as an amidating agent, again at a high temperature (220 °C) with a long reaction time (15 h).[41] However, Sun *et al.* reported a bioinorganic nanohybrid catalyst for acetaminophen synthesis in 10 min with a 96% yield.[24] However, it was a combination of oligomeric esterase and expensive platinum nanoparticles.

We attempted to synthesize acetaminophen using relatively inexpensive nZVI without using any organic solvent or any

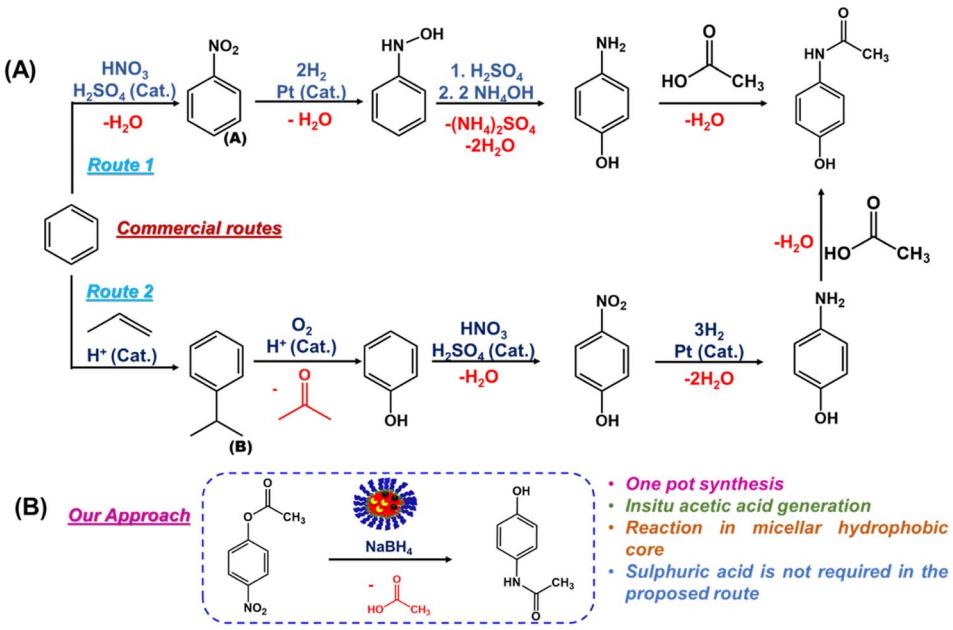

Fig. 7 (A) Commercial routes for acetaminophen synthesis. (B) Our approach for the direct synthesis of acetaminophen.

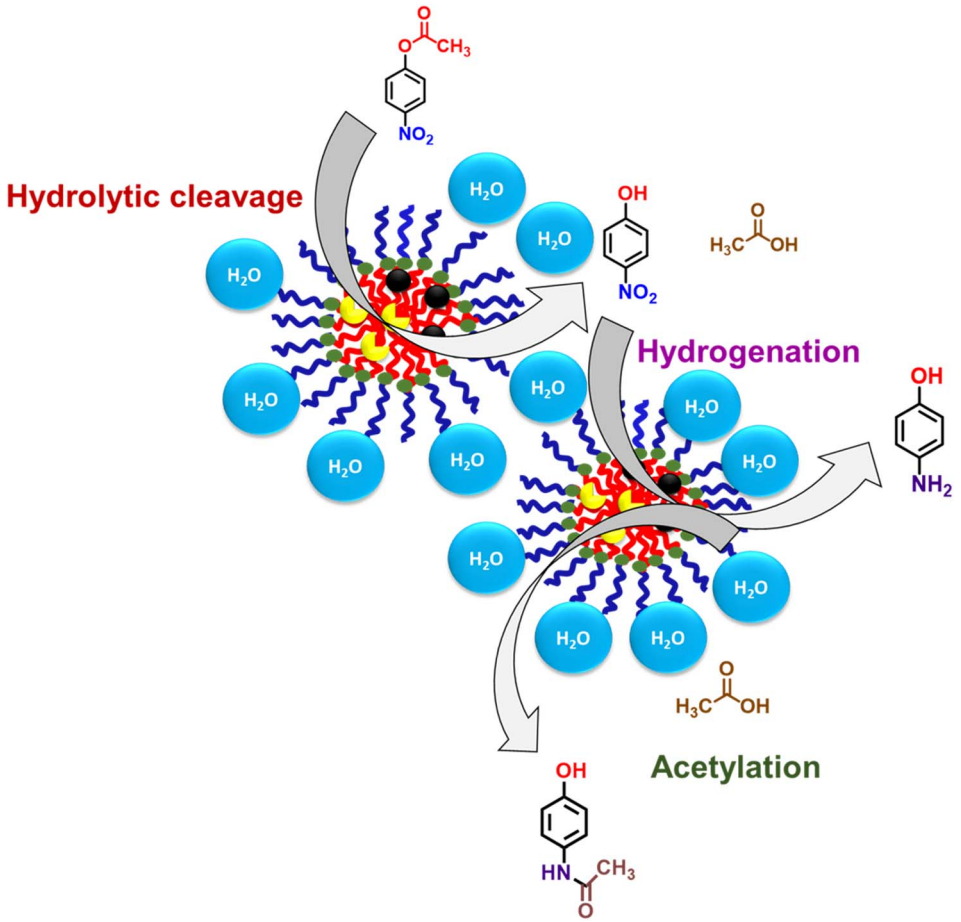

Scheme 3 Plausible mechanism for the direct synthesis of acetaminophen using *p*-nitrophenyl acetate as a reactant in the nanomicellar core.

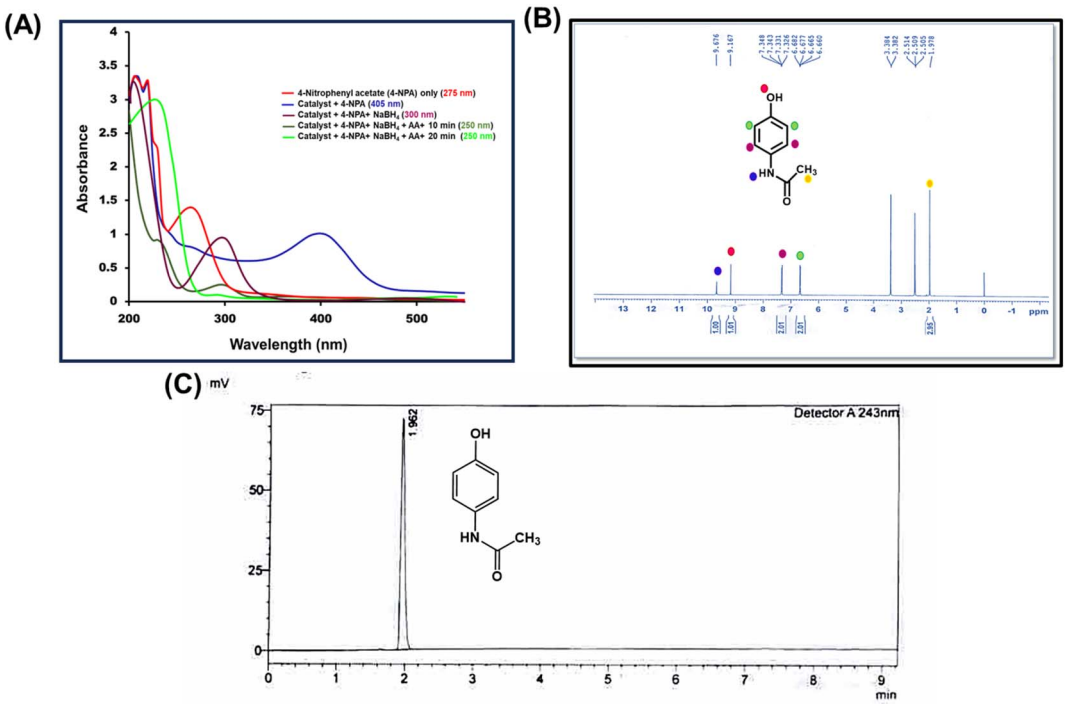

Fig. 8 Chemoenzymatic synthesis of acetaminophen in one pot using nanoreactors. The product was confirmed by (A) UV-visible spectroscopy, (B) NMR and (C) HPLC. (Reaction conditions: *p*-NPA (1 mM, nanoreactors (2 mL contains nZVI (18 wt%), $NaBH_4$ (1.4 mM) at 35 °C). λ_{max} of *p*-NPA (275 nm, red), *p*-NP (405 nm, blue), *p*-AP (312 nm, brown), and acetaminophen (243 nm, green).

harsh mineral acid. When the aqueous solution of nanoreactor nZVI-CALB@NM was incubated with *p*-nitrophenyl acetate and $NaBH_4$, the final product, acetaminophen, was spontaneously formed in the reaction flask (Scheme 3). The entire synthesis was performed in one pot at room temperature without any specialized equipment. The progress of the reaction was monitored using UV-visible spectrophotometry. The reaction was initiated in an aqueous phase, and subsequent hydrolysis of *p*-NPA by nZVI-CALB@NM yielded *p*-NP as an intermediate, characterized by the development of a yellow colour in the solution (Fig. 8).

It is noteworthy that acetic acid was released as a byproduct of hydrolysis. Subsequent reduction of *p*-NP was marked by the disappearance of the yellow colour under reducing reaction conditions, showing that this two-step reaction was completed by a single nanoreactor platform. The reduced product, *p*-AP, undergoes acetylation when subsequently reacted with acetic acid (released during the hydrolysis step) in the nanoreactors to form the final product, acetaminophen. The whole reaction process was completed within 30 min, and no spectral change was observed after 30 min of the reaction.

There is an additional advantage to the above reaction. The weakly acidic environment generated due to the release of acetic acid during hydrolysis favours acetylation without the use of any additional organic solvent or harsh acid. For the same reasons, the whole cascade process occurred in a single pot, and isolation of products and byproducts is not necessary before acetylation.

The acetaminophen isolated after the complete cascade cycle was characterized by analytical techniques, such as NMR, FT-IR and MS analysis (Fig. 8(B) and S19, S20†). To quantify the final product, *i.e.*, acetaminophen, HPLC analysis was carried out and showed a 99.2% conversion yield (Fig. 8(C)). All the analyses confirmed the formation of acetaminophen as the single product from *p*-nitrophenylacetate. The peak matched with standard acetaminophen, and the HPLC spectra are shown in Fig. S21.† This technique makes it easier to produce pharmaceutically active molecules in a set up where funding for a new production line or access to equipment is limited. Such processes are likely to benefit the pharmaceutical sector, resulting in significant cost reductions.

3.7 Recycling studies

The catalytic nanoreactors demonstrate another advantage, *i.e.*, recyclability. It was also established from the recycling experiments that catalytic activity did not decrease even after multiple cycles, and the nanoreactors were very stable for 5 cycles (Fig. 9). After the reaction completion, nZVI-CALB@NM was separated from the reaction mixture *via* simple extraction with chloroform. The product was analyzed by UV-visible spectrophotometry. HR-TEM imaging of the recycled nanoreactors after the 5th cycle showed a change in micellar morphology and slight agglomeration of zerovalent iron nanoparticles (Fig. 9(A) and (B)). FE-SEM analysis also suggested that the aggregation of nanomicelles was initiated (Fig. 9(C)). FTIR analysis confirms the presence of a peak corresponding to amide, and urethane in the recycled catalysts confirms that the chemical structure of nanoreactors remains intact (Fig. 9(D)). The recycling results supported the robust nature of the nanoreactors (Fig. 9(E)).

Leaching and deactivation of the catalyst have a cause–effect relationship.[43] To confirm that no leaching occurred, we dialyzed the reaction mixture using a dialysis membrane with

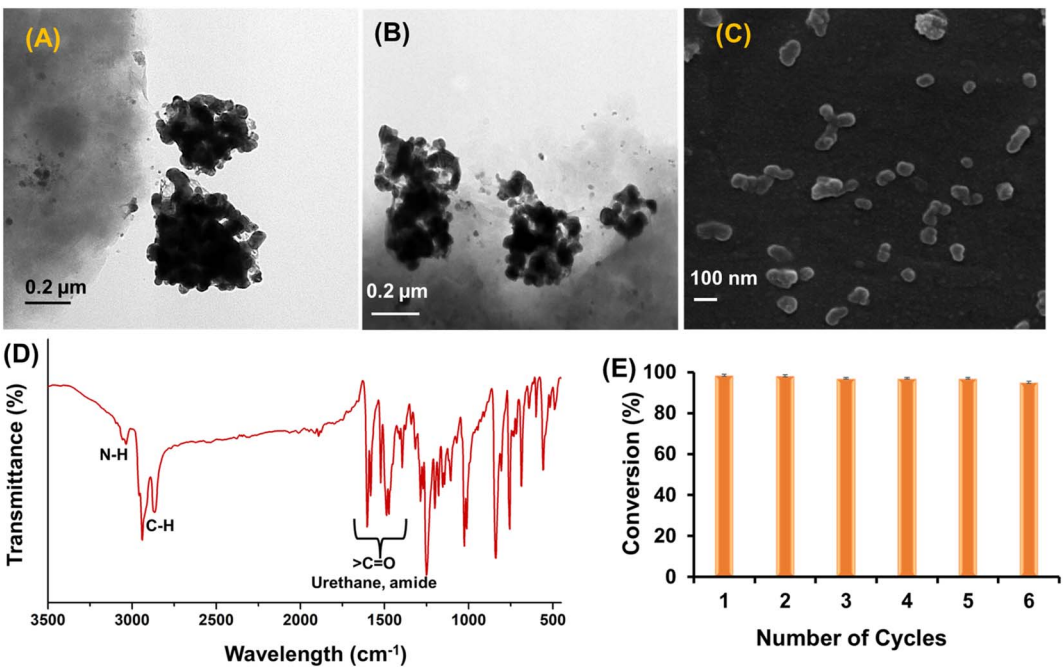

Fig. 9 Characterization of the recycled catalyst: (A and B) HR-TEM images after 5th catalytic cycle (C) FEG-SEM analysis, (D) FT-IR analysis and (E) recycling study (error bar less than 1 standard deviation ($n = 3$)).

a 3500 Da molecular weight cut off. It was confirmed from the ICP-AES analysis that no Fe ions could be detected in the dialysis solvent. This supports the fact that no leaching occurred in the current experimental setup.

3.8 Plausible mechanism

A plausible mechanism was proposed to explain the steps of cascade catalysis occurring inside the nanoreactors in water, as shown in Scheme 3. nZVI-CALB@NM act as catalytic nanoreactors that entrap the reactants by virtue of hydrophobic interactions; thus, the cascade can be carried out in water instead of organic solvents.[19] The fluorescence microscopy image of hydrophobic dye (*i.e.*, pyrene) encapsulated in micelles provides evidence of their ability to entrap hydrophobic moieties (Fig. 2). The nanoreactors contain CALB and zerovalent iron nanoparticles.

The cascade reaction consists of two sequential steps: hydrolysis and reduction. The hydrolysis step was catalyzed by CALB, and the reduction step was catalyzed by nZVI synergistically in the hydrophobic core of nanomicelles to achieve the final product in the single pot.[19–21] The catalytic activity results from the formation of a substrate–catalyst complex through hydrophobic interaction.[44] Due to the confinement of both the enzyme and nZVI in the nanomicellar hydrophobic core, the hydrophobic reactant molecules come in close proximity to the enzyme and nZVI. The high surface area of the iron nanoparticles, better dispersibility of CALB–nZVI in the core and the nanostructure of nZVI in the nZVI-CALB@NM might contribute to the high catalytic activity. Herein, the generation of acetic acid *in situ* during hydrolysis of *p*-NPA maintains a weakly acidic medium and further facilitates the next acetylation step to yield acetaminophen as the final product.

In our approach, the catalyst is developed from the non-toxic precursors and the earth abundant iron. Moreover, the stability and recyclability of enzymes and nZVI are enhanced due to entrapment in nanomicelles. In comparison to traditional methods for synthesizing acetaminophen, the present strategy offers several advantages, including reduced costs, minimized time requirements, and lower environmental impact. Notably, all reactions were executed in an aqueous phase under ambient conditions, without any specialized equipment. These factors support the feasibility of the catalyst for the scaleup synthesis of acetaminophen.

4 Conclusion

A novel amphiphilic polymer was successfully synthesized by the functionalization of tyrosine with polyethylene glycol and undecanoic acid. The amphiphilic polymer was successfully self-assembled into the nanomicelles. A low CMC value of 0.97 mg L^{-1} indicated the high stability of the nanomicelles. The hydrophobic core of the nanomicelles encapsulated the enzymes CALB and nZVI to obtain catalytic nanoreactors for the chemoenzymatic synthesis of *p*-aminophenol from *p*-nitrophenylesters. Under optimized conditions, the rationally designed catalytic nanoreactors facilitate the entire cascade reaction in water under ambient conditions. To demonstrate the robust nature of the nanoreactors, a series of *p*-nitrophenyl ester derivatives were used as reactants for the cascade reactions. The corresponding *p*-aminophenol was obtained as the desired product under mild reaction conditions in less time. An environmentally benign chemoenzymatic cascade reaction was proposed for the multistep catalytic synthesis of acetaminophen from *p*-nitrophenyl acetate. The acetic acid generated *in situ* during the hydrolysis step provides a mild acidic condition for the synthesis of acetaminophen. This process is free of the usage of toxic solvents, expensive metals and hazardous acid, and the final product was obtained in high yield within 30 min. The isolated acetaminophen was characterized using ^{1}H NMR, FTIR and ESI-MS spectroscopic techniques.

Finally, the operational recyclability showed no significant loss in activity up to 5 consecutive cascade cycles of use at 35 °C. The easy magnetic recovery and reusability of the catalytic nanoreactors are critical for their application in scale-up processes. In this work, we propose a novel method to heterogenise enzymes and house them with metal nanoparticles in nanomicelles to catalyse novel cascade industrial manufacturing processes. These findings also imply that similar results can be anticipated for other enzymatic processes and sequential cascade catalysis.

Abbreviations

CALB@NM	CALB-loaded nano micelles
nZVI-CALB@NM	Zerovalent iron nanoparticles CALB-loaded nanomicelles

Data availability

The authors declare that the data supporting the findings of this study are available within the paper and its ESI file.† If any raw data files are needed in another format, they are available from the corresponding author upon reasonable request.

Author contributions

Falguni Shukla: investigation, formal analysis, methodology, writing, review & editing, visualization. Dilraj Singh: investigation, formal analysis, methodology. Sonal Thakore: conceptualization, supervision, project administration, data curation, writing – review & editing, funding acquisition.

Conflicts of interest

There are no conflicts to declare.

Acknowledgements

The authors acknowledge DST-SERB Power Grant (SPG/2021/0003149) for financial support and DST-FIST, Department of Chemistry, for the NMR facility. FS acknowledges University

Research Fellowship. The authors are grateful to SAIF-IIT Mumbai for HRTEM as well as FESEM, CSIR CLRI for AFM analysis, MNIT Jaipur for DLS, Zeta Potential, XPS analysis, IIT Madras for VSM analysis and IIT Gandhinagar for CD analysis.

References

1 R. D. Lewis, S. P. France and C. A. Martinez, Emerging Technologies for Biocatalysis in the Pharmaceutical Industry, *ACS Catal.*, 2023, **13**, 5571–5577, DOI: **10.1021/acscatal.3c00812**.

2 W. Liang, P. Wied, F. Carraro, C. J. Sumby, B. Nidetzky, C. K. Tsung, P. Falcaro and C. J. Doonan, Metal-Organic Framework-Based Enzyme Biocomposites, *Chem. Rev.*, 2021, **121**, 1077–1129, DOI: **10.1021/acs.chemrev.0c01029**.

3 Y. Liu, P. Liu, S. Gao, Z. Wang, P. Luan, J. González-Sabín and Y. Jiang, Construction of chemoenzymatic cascade reactions for bridging chemocatalysis and Biocatalysis: Principles, strategies and prospective, *Chem. Eng. J.*, 2021, **420**, 127659, DOI: **10.1016/j.cej.2020.127659**.

4 Z. Qin, N. Feng, Y. Ma, Y. Li, L. Xu, Y. Wang, X. Fei and J. Tian, A lipase/poly (ionic liquid)-styrene microspheres/PVA composite hydrogel for esterification application, *Enzyme Microb. Technol.*, 2022, **152**, 109935, DOI: **10.1016/j.enzmictec.2021.109935**.

5 A. Rodriguez-Abetxuko, D. Sánchez-deAlcázar, P. Muñumer and A. Beloqui, Tunable Polymeric Scaffolds for Enzyme Immobilization, *Front. Bioeng. Biotechnol.*, 2020, **8**, 1–27, DOI: **10.3389/fbioe.2020.00830**.

6 X. Liu, H. Luo, D. Yu, J. Tan, J. Yuan and H. Li, Synthetic biology promotes the capture of CO2 to produce fatty acid derivatives in microbial cell factories, *Bioresour. Bioprocess.*, 2022, **9**, 124, DOI: **10.1186/s40643-022-00615-2**.

7 Y. Liu, L. Song, N. Feng, W. Jiang, Y. Jin and X. Li, Recent advances in the synthesis of biodegradable polyesters by sustainable polymerization: lipase-catalyzed polymerization, *RSC Adv.*, 2020, **10**, 36230–36240, DOI: **10.1039/d0ra07138b**.

8 C. Ortiz, M. L. Ferreira, O. Barbosa, J. C. S. Dos Santos, R. C. Rodrigues, Á. Berenguer-Murcia, L. E. Briand and R. Fernandez-Lafuente, Novozym 435: the "perfect" lipase immobilized biocatalyst?, *Catal. Sci. Technol.*, 2019, **9**, 2380–2420, DOI: **10.1039/c9cy00415g**.

9 J. M. Palomo, *Chem. Commun.*, 2019, **55**, 9583–9589, DOI: **10.1039/C9CC04944D**.

10 J. M. Naapuri, N. Losada-Garcia, J. Deska and J. M. Palomo, Synthesis of silver and gold nanoparticles-enzyme-polymer conjugate hybrids as dual-activity catalysts for chemoenzymatic cascade reactions, *Nanoscale*, 2022, **14**, 5701–5715, DOI: **10.1039/d2nr00361a**.

11 X. Li, X. Cao, J. Xiong and J. Ge, Enzyme–Metal Hybrid Catalysts for Chemoenzymatic Reactions, *Small*, 2020, **16**, 1–14, DOI: **10.1002/smll.201902751**.

12 A. Rodriguez-Abetxuko, P. Muñumer, M. Okuda, J. Calvo, M. Knez and A. Beloqui, Nanoconfined (Bio)Catalysts as Efficient Glucose-Responsive Nanoreactors, *Adv. Funct. Mater.*, 2020, **30**, 1–10, DOI: **10.1002/adfm.202002990**.

13 G. Gahlawat and A. R. Choudhury, A review on the biosynthesis of metal and metal salt nanoparticles by microbes, *RSC Adv.*, 2019, **9**, 12944–12967, DOI: **10.1039/c8ra10483b**.

14 G. Kozma, A. Rónavári, Z. Kónya and Á. Kukovecz, Environmentally Benign Synthesis Methods of Zero-Valent Iron Nanoparticles, *ACS Sustain. Chem. Eng.*, 2016, **4**, 291–297, DOI: **10.1021/acssuschemeng.5b01185**.

15 R. Benavente, D. Lopez-Tejedor and J. M. Palomo, Synthesis of a superparamagnetic ultrathin FeCO3 nanorods-enzyme bionanohybrid as a novel heterogeneous catalyst, *Chem. Commun.*, 2018, **54**, 6256–6259, DOI: **10.1039/c8cc02851f**.

16 P. Nariya, M. Das, F. Shukla and S. Thakore, Synthesis of magnetic silver cyclodextrin nanocomposite as catalyst for reduction of nitro aromatics and organic dyes, *J. Mol. Liq.*, 2020, **300**, 112279, DOI: **10.1016/j.molliq.2019.112279**.

17 F. Shukla, T. Kikani, A. Khan and S. Thakore, α-Hydroxy acids modified β-cyclodextrin capped iron nanocatalyst for rapid reduction of nitroaromatics: a sonochemical approach, *Int. J. Biol. Macromol.*, 2022, **209**, 1504–1515, DOI: **10.1016/j.ijbiomac.2022.04.149**.

18 S. Gao, Y. Liu, L. Wang, Z. Wang, P. Liu, J. Gao and Y. Jiang, Incorporation of metals and enzymes with porous imine molecule cages for highly efficient semiheterogeneous chemoenzymatic catalysis, *ACS Catal.*, 2021, **11**, 5544–5553, DOI: **10.1021/acscatal.1c00587**.

19 M. Cortes-Clerget, N. Akporji, J. Zhou, F. Gao, P. Guo, M. Parmentier, F. Gallou, J. Y. Berthon and B. H. Lipshutz, Bridging the gap between transition metal- and bio-catalysis via aqueous micellar catalysis, *Nat. Commun.*, 2019, **10**, 1–10, DOI: **10.1038/s41467-019-09751-4**.

20 F. Shukla, M. Das and S. Thakore, Copper nanoparticles loaded polymer vesicles as environmentally amicable nanoreactors: a sustainable approach for cascading synthesis of benzimidazole, *J. Mol. Liq.*, 2021, **336**, 116217, DOI: **10.1016/j.molliq.2021.116217**.

21 R. R. Thakore, B. S. Takale, G. Casotti, E. S. Gao, H. S. Jin and B. H. Lipshutz, Chemoselective Reductive Aminations in Aqueous Nanoreactors Using Parts per Million Level Pd/C Catalysis, *Org. Lett.*, 2020, **22**, 6324–6329, DOI: **10.1021/acs.orglett.0c02156**.

22 G. Graziano, Solving a solubility problem, *Nat. Rev. Chem.*, 2020, **4**, 332, DOI: **10.1038/s41570-020-0202-3**.

23 Q. Geng and J. Du, Reduction of 4-nitrophenol catalyzed by silver nanoparticles supported on polymer micelles and vesicles, *RSC Adv.*, 2014, **4**, 16425–16428, DOI: **10.1039/c4ra01866d**.

24 B. H. San, S. Ravichandran, K. S. Park, V. K. Subramani and K. K. Kim, Bioinorganic Nanohybrid Catalyst for Multistep Synthesis of Acetaminophen, an Analgesic, *ACS Appl. Mater. Interfaces*, 2016, **8**, 30058–30065, DOI: **10.1021/acsami.6b12875**.

25 S. S. Nadar and V. K. Rathod, Encapsulation of lipase within metal-organic framework (MOF) with enhanced activity intensified under ultrasound, *Enzyme Microb. Technol.*, 2018, **108**, 11–20, DOI: **10.1016/j.enzmictec.2017.08.008**.

26 M. Das, A. Joshi, R. Devkar, S. Seshadri and S. Thakore, Vitamin-H Channeled Self-Therapeutic P-gp Inhibitor Curcumin-Derived Nanomicelles for Targeting the Tumor Milieu by pH- and Enzyme-Triggered Hierarchical Disassembly, *Bioconjug. Chem.*, 2022, **33**, 369–385, DOI: **10.1021/acs.bioconjchem.1c00614**.

27 R. Tao, M. Gao, F. Liu, X. Guo, A. Fan, D. Ding, D. Kong, Z. Wang and Y. Zhao, Alleviating the Liver Toxicity of Chemotherapy via pH-Responsive Hepatoprotective Prodrug Micelles, *ACS Appl. Mater. Interfaces*, 2018, **10**, 21836–21846, DOI: **10.1021/acsami.8b04192**.

28 S. Imai, M. Takenaka, M. Sawamoto and T. Terashima, Self-Sorting of Amphiphilic Copolymers for Self-Assembled Materials in Water: Polymers Can Recognize Themselves, *J. Am. Chem. Soc.*, 2019, **141**, 511–519, DOI: **10.1021/jacs.8b11364**.

29 N. U. Deshpande and M. Jayakannan, Cisplatin-Stitched Polysaccharide Vesicles for Synergistic Cancer Therapy of Triple Antagonistic Drugs, *Biomacromolecules*, 2017, **18**, 113–126, DOI: **10.1021/acs.biomac.6b01411**.

30 R. Aluri, S. Saxena, D. C. Joshi and M. Jayakannan, Multistimuli-Responsive Amphiphilic Poly(ester-urethane) Nanoassemblies Based on l-Tyrosine for Intracellular Drug Delivery to Cancer Cells, *Biomacromolecules*, 2018, **19**, 2166–2181, DOI: **10.1021/acs.biomac.8b00334**.

31 Z. Zhang, X. Chen, X. Gao, X. Yao, L. Chen, C. He and X. Chen, Targeted dextran-b-poly(ε-caprolactone) micelles for cancer treatments, *RSC Adv.*, 2015, **5**, 18593–18600, DOI: **10.1039/c4ra15696j**.

32 N. G. Patil, N. B. Basutkar and A. V. Ambade, Copper and silver nanoparticles stabilized by bistriazole-based dendritic amphiphile micelles for 4-nitrophenol reduction, *New J. Chem.*, 2017, **41**, 4546–4554, DOI: **10.1039/c7nj00605e**.

33 M. Li, M. Gao, Y. Fu, C. Chen, X. Meng, A. Fan, D. Kong, Z. Wang and Y. Zhao, Acetal-linked polymeric prodrug micelles for enhanced curcumin delivery, *Colloids Surf. B Biointerfaces*, 2016, **140**, 11–18, DOI: **10.1016/j.colsurfb.2015.12.025**.

34 S. Dinda, M. Ghosh and P. K. Das, Spontaneous Formation of a Vesicular Assembly by a Trimesic Acid Based Triple Tailed Amphiphile, *Langmuir*, 2016, **32**, 6701–6712, DOI: **10.1021/acs.langmuir.6b01942**.

35 L. Piñeiro, M. Novo and W. Al-Soufi, Fluorescence emission of pyrene in surfactant solutions, *Adv. Colloid Interface Sci.*, 2015, **215**, 1–12, DOI: **10.1016/j.cis.2014.10.010**.

36 Y. Zhong, W. Yang, H. Sun, R. Cheng, F. Meng, C. Deng and Z. Zhong, Ligand-directed reduction-sensitive shell-sheddable biodegradable micelles actively deliver doxorubicin into the nuclei of target cancer cells, *Biomacromolecules*, 2013, **14**, 3723–3730, DOI: **10.1021/bm401098w**.

37 D. Šmejkalová, K. Nešporová, G. Huerta-Angeles, J. Syrovátka, D. Jirák, A. Gálisová and V. Velebný, Selective in vitro anticancer effect of superparamagnetic iron oxide nanoparticles loaded in hyaluronan polymeric micelles, *Biomacromolecules*, 2014, **15**, 4012–4020, DOI: **10.1021/bm501065q**.

38 S. Zhu, S. H. Ho, X. Huang, D. Wang, F. Yang, L. Wang, C. Wang, X. Cao and F. Ma, Magnetic Nanoscale Zerovalent Iron Assisted Biochar: Interfacial Chemical Behaviors and Heavy Metals Remediation Performance, *ACS Sustain. Chem. Eng.*, 2017, **5**, 9673–9682, DOI: **10.1021/acssuschemeng.7b00542**.

39 D. Mandal, M. Ghosh, S. Maiti, K. Das and P. K. Das, Water-in-oil microemulsion doped with gold nanoparticle decorated single walled carbon nanotube: scaffold for enhancing lipase activity, *Colloids Surfaces B Biointerfaces*, 2014, **113**, 442–449, DOI: **10.1016/j.colsurfb.2013.09.047**.

40 Z. Li, Y. Ding, X. Wu, J. Ge, P. Ouyang and Z. Liu, RSC Advances prepared from disassembly of an enzyme, *RSC Adv.*, 2016, **6**, 20772–20776, DOI: **10.1039/C5RA27904F**.

41 R. Joncour, N. Duguet, E. Métay, A. Ferreira and M. Lemaire, Amidation of phenol derivatives: A direct synthesis of paracetamol (acetaminophen) from hydroquinone, *Green Chem.*, 2014, **16**, 2997–3002, DOI: **10.1039/c4gc00166d**.

42 P. Gopinathan, S. Gopinathan, C. Kuruvilla, J. Pardhy and S. A. Ratnasamy, Process for the preparation of N-acetyl aminophenols, *US Pat.*, US5856575A, 1999, pp. 3–6.

43 I. Sádaba, M. L. Granados, A. Riisagerc and E. Taarninga, Deactivation of solid catalysts in liquid media: the case of leaching of active sites in biomass conversion reactions, *Green Chem.*, 2015, **17**, 4133–4145, DOI: **10.1039/b000000x**.

44 L. R. Lawin, W. K. Fife and C. X. Tian, Hydrolysis of p-nitrophenyl esters in the presence of polymer micelles. Selectivity and biphasic behavior with increasing ester concentration, *Langmuir*, 2000, **16**, 3583–3587, DOI: **10.1021/la980486l**.